Journal of Sound and Vibration (1999) **220**(3), 469–496
Article No. jsvi.1998.1954, available online at http://www.idealibrary.com on IDEAL

ACTIVE CONTROL OF ENVIRONMENTAL NOISE, III: IMPLEMENTATION OF THEORY INTO PRACTICE

S. E. WRIGHT AND B. VUKSANOVIC

School of Engineering, *University of Huddersfield*, *Huddersfield HD*1 3*DH*, *UK*

(*Received* 1 *December* 1997, *and in final form* 3 *September* 1998)

In paper I [1] a theory for generating electronically controlled acoustic shadows for environmental noise reduction was considered. In paper II [2] the theory was extended to complex high frequency sound from non compact sources. Finally paper IV [10] considers the practical applications of the theory. These studies show that deep shadows are theoretically possible. This paper considers the implementation of the theory into a practical multichannel free-field control system and its basic performance. Providing certain stability conditions are met, deep shadows > 60 dB are generated at the microphones, limited only by the ambient noise of the laboratory.

1. INTRODUCTION

At the outset of this study, there was daunting advice from the 'experts' that, from their experience, particularly in enclosures, active noise control in unrestricted space would be a formidable task. Their investigations revealed that sound reductions hardly reached double figures (in dB's): the higher the frequency, the less the reduction, both in region size and attenuation depth. Then for outdoor non-compact (large) sources, there was the additional problem of requiring large multi-channel systems, which from a stability point of view, 'could fall apart'.

Well, this appeared to be the situation. However, most of the outdoor studies were *ad hoc*, applied to a particular environment, with little knowledge of the acoustics or control strategies envolved. It was decided therefore, to build a special purpose facility to establish the basic performance of free-field active noise control (ANC) systems, under strict laboratory controlled conditions, and to establish how close hardware systems could perform compared to the theoretical predictions [1], [2] and [10].

Active Noise Control is reducing noise by cancelling it with a negative replica (antisound). Much of the past work in this area has been applied to noise reduction in confined spaces, such as ducts and enclosures. The aim of the present work is to investigate systematically ANC methods for outdoor applications, through the development of freefield electronically controlled acoustic shadow (ECAS) systems, as illustrated in Figure 1.

0022–460X/99/080469 + 28 $30.00/0

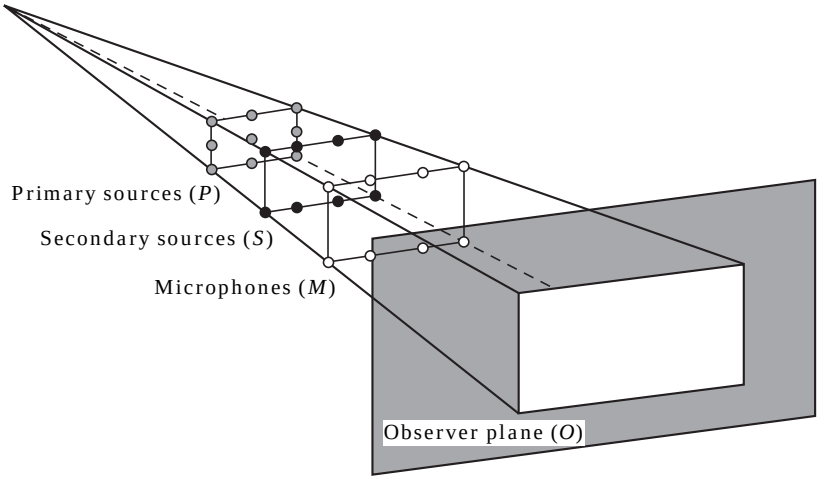

Figure 1. Electronically controlled acoustic shadow (ECAS) system.

The resulting shadows are predicted to be superior to conventional shadows produced in nature by solid boundaries. This is made possible through the cancelling secondary sources having intelligence, adjusting their strengths automatically to produce the optimum shadow. A conventional solid boundary can attempt only to return the sound pressure evenly across its surface. This results in a non-optimum shadow, with sound leakage through diffraction effects from around the body edges. Thus the impressive performance of the Electronically Controlled Acoustic Shadow system, gave considerable motivation to establish if a practical implementation of the theory into hardware would be possible.

The following investigation describes the appropriate hardware necessary to establish the basic system performance, and the control schemes necessary to produce deep shadows. The paper is not an exhaustive study of control strategies, nor a plethora of experimental data. This is a subject for further publications. However, sufficient data is given to varify a successful practical demonstration.

2. THEORY INTO PRACTICE

2.1. BASIC CONSIDERATIONS

Normally, industrial control systems are electrically compact, where the system size is small compared with the electrical disturbance wavelength. Here the plant response is dominated by time and phase delays caused by the lumped electrical and mechanical components within the system. However, in acoustical plants the acoustic wavelength is often smaller than the physical system size to be controlled. In this case the plant is considered non-compact or spatially distributed. Here the acoustic system response is dominated by the disturbance propagation times within the plant. In our application, the dominant plant is the free-field propagation matrix between the secondary sources and microphones.

Physically, cancelling sound in free field (large unrestricted space) is quite different from cancelling sound in enclosures. This results in quite a different plant to control. The cancelling secondary sound within confined spaces, for example, is not usually travelling in the same direction as the primary sound; it is also usually diffuse, sometimes resonant. In this case the resulting cancellation area (quiet zone) is confined to within a fraction of a wavelength of the detector.

However, it is not generally understood that, for progressive fields and successive alignment of the primary sources, secondary sources and error detectors, the quiet zone can extend to infinity, or at least to large distances, no matter what the frequency. This makes the plant, in some ways, potentially more controllable than enclosed fields, and high frequency noise reduction a more realistic possibility by using this technique. In control terms, the free-field plant has unique characteristics, with its own sets of eigenvalues, stability, convergence and error criteria.

2.2. SYSTEM STABILITY

In any useful control system the plant has to be stable. In this application, the stability of the free-field plant will depend primarily on the propagation free-field path delays and on the combined electro-mechanical transfer function of the system (filters, amplifiers, loudspeakers and microphones). Rather than attempt to investigate the stability of complex primary sound cancellation in general, in the time domain, it was considered more instructive, initially, to establish the basic discrete frequency performance in the frequency domain. Correspondingly, rather than using the filtered $\times$ algorithm, and 'long' finite impulse response (FIR) filters, the stability and adaptive performance, is investigated by using the basic delayed least mean square (LMS) algorithm, and monochromatic two tap FIR filters.

For the system to be stable, the phase around each of the individual adaptive loops, at any frequency, should be close to a multiple of 2π radians. It is found that many stability regions can exist for a given frequency, whose position and number can be selected through altering the sample delay in the LMS algorithm. For optimum adaptive performance, in terms of convergence speed, shadow depth and harmonic distortion, it is essential for each of these adaptive loops to operate close to the centre of its stability region, and all stability regions to be aligned at the frequency of interest.

A further condition needed for multichannel systems to converge effectively is that the transfer function of the multi-channel plant, governed by the free-field propagation matrix, should be robustly stable. The robustness of this system is investigated by using, firstly, conventional control condition methods, and secondly, by a novel sum and difference acoustic theory. Robustness is expressed in the frequency domain through the concept of condition spectra, where it is found that the free-field propagation matrix has multiple condition peaks. Providing these peaks are avoided and other stability criteria are met, system convergence should be assured.

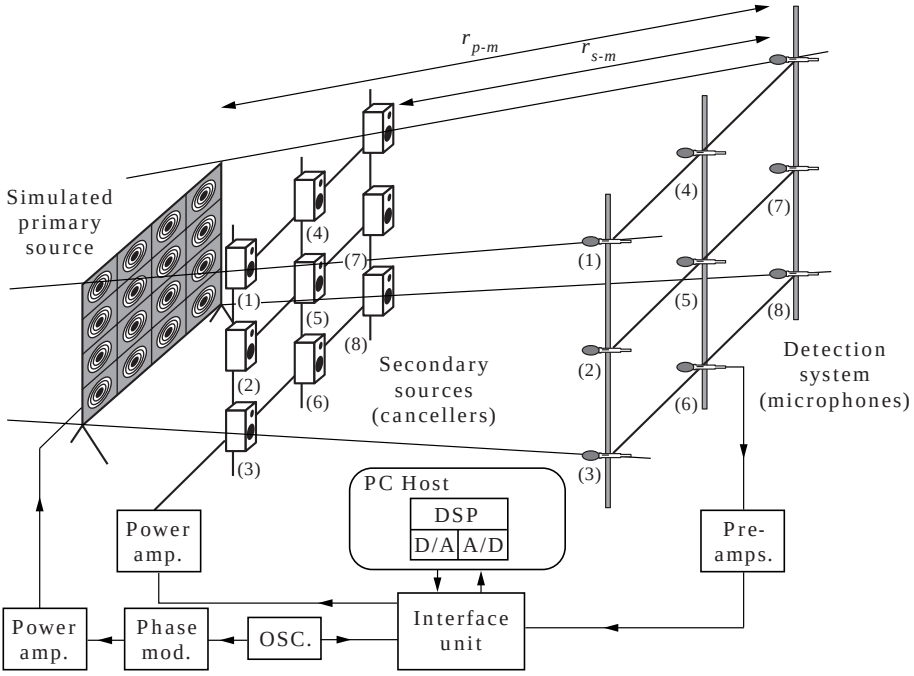

Figure 2. ECAS laboratory system.

2.3. EXPERIMENTAL FACILITY

Detailed analysis predicts that deep shadows (>120 dB) are possible, indicating that practical shadows (>20 dB) are potentially achievable.

The task now is to build a practical free-field system and establish its basic performance. A purpose built anechoic facility $6\,\text{m} \times 6\,\text{m} \times 5\,\text{m}$ has been constructed at the University of Huddersfield and free-field systems implemented into hardware as illustrated in Figure 2 and Figure 3. The eight channel system is based on the Texas Instruments TMS320C32 processor using a 2 tap FIR filter and a circular buffer technique to implement the delayed version of the LMS update algorithm. This allows easy algorithm implementation in software and significantly reduces computation time for large channel number systems.

A 16 input 8 output AD/DA board PC16IO8 provides a 12 bit interface with external equipment. The board contains three selectable levels of gain 1, 10 and 100. The cancelling stereo loudspeakers (secondary sources) are each 20 W containing their own power amplifiers and power supplies (in pairs); their frequency response is 32 Hz to 20 kHz. The stereo preamplifiers have a fixed gain of approximately 100 and a frequency response of 30 Hz to 15 kHz; they are battery powered. The simulated primary source is constructed from sixteen 8 inch, 20 W loudspeakers. These are mounted on a 1 m square baffle powered from a 120 W power amplifier. There is a provision to drive individual banks of speakers with relative phase variation

2.4. BASIC CONTROL SYSTEM

Figure 4 shows a schematic diagram of a general adaptive control system. X is the sound from the primary noise source. P is the primary propagation path to the cancelling point, where the sound arrives as D. In the lower path, W is a weight adjustment filter which modifies a copy of X to Y. The sound is then modified as it propagates along the cancelling path C where it becomes Y' at the cancelling point.

The sounds from the primary and cancelling paths are monitored at the cancelling point; the error E between them is then used to adjust W via the LMS algorithm to make Y' equal but opposite to D. This process continues until E goes to zero. $\hat{C}$ is a copy of C which allows performance flexibility implemented through the LMS algorithm.

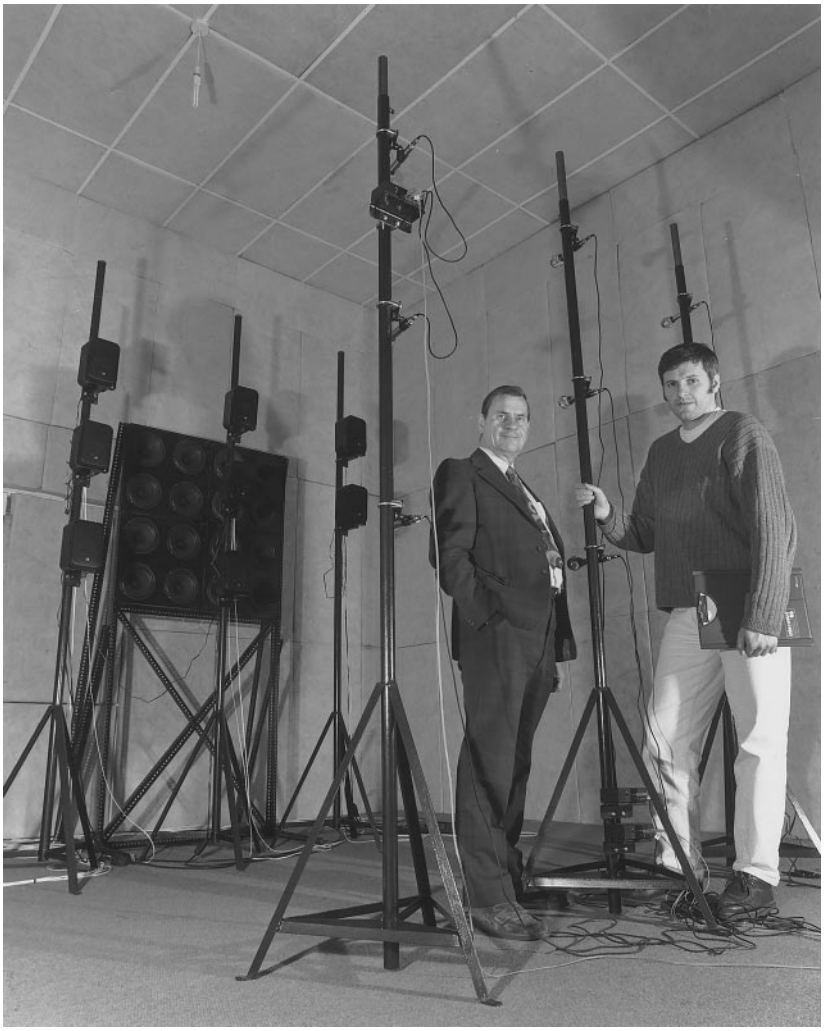

Figure 3. ECAS facility picture.

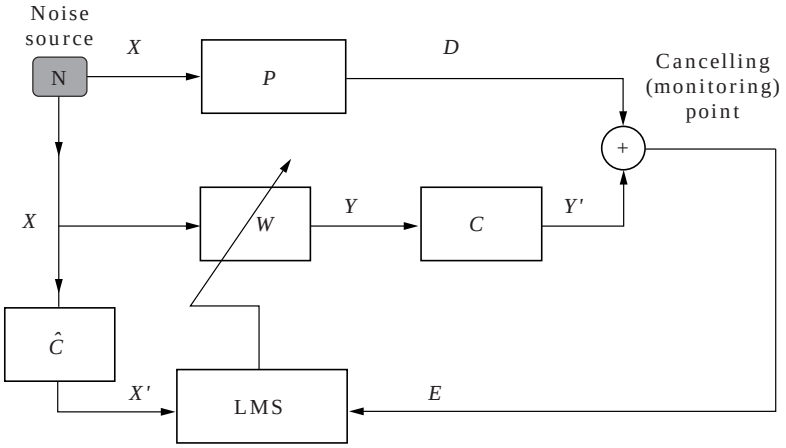

Figure 4. Basic control system.

2.5. TIME DOMAIN

The main steps in the adaptive process for a multi-channel system are given below; for brevity the theory is given in a simplified form. More rigorous and therefore necessarily extensive mathematical treatments, for example, can be found in references [3–6]. Each step in the process is executed at each sampling time step (sample number n not indicated).

$$E = D + Y', \tag{1}$$

$$Y' = C * Y, \qquad Y = X^{\mathrm{T}}W, \tag{2}$$

$$C = \begin{bmatrix} C_{11} & C_{12} & \cdot & \cdot & C_{1s} \\ C_{21} & \cdot & & & \\ \cdot & & \cdot & & \\ \cdot & & & \cdot & \\ C_{m1} & \cdot & \cdot & \cdot & C_{ms} \end{bmatrix}, \tag{3}$$

$$E = D + C * (X^{\mathrm{T}}W). \tag{4}$$

W is adjusted until

$$C * (X^{\mathrm{T}}W) \rightarrow -D \qquad \text{making } E \rightarrow 0. \tag{5}$$

Traditionally, in control theory, the error is usually given as the difference between D and Y'. However, in acoustic systems, the error detectors (microphones) can physically only add these components.

For a multichannel ANC system with m error microphones and s secondary sources, the error vector between $D_{m\times 1}$ and $Y'_{m\times 1}$ for all microphones, is $E = E_{m\times 1}$. The vector $Y'_{m\times 1} = Y'_{s\times 1}$ represents the summation of signals at each of the microphones, from all the secondary sources, after being modified by the propagation matrix $C = C_{m\times s}$, i.e., $Y'_m = \Sigma_s\, Y_s\, C_{ms}$. The propagation matrix

elements C_{ms} are the impulse response functions between the microphones (m) and secondary sources (s). The vector $Y = Y_{s\times 1}$ is the output to the secondary sources from the reference signal X, after being modified by the filter weights W, i.e., $Y_s = XW_s$. The matrix $X = X_{s\times s}$ is a diagonal matrix of s reference noise signals. For a common reference all elements are equal. T indicates the transpose of X, and the operation $*$ denotes linear convolution.

The cost function that is minimized in the adaptive process is the sum of mean squared errors ξ from all microphones m. If the signal character is varying slowly compared with the sampling time, then the instantaneous squared error can be used to estimate the mean squared error given by

$$\xi = \sum_{m=1}^{M} E_m^2 = E^T E. \tag{6}$$

The algorithm that is used to control the adaptive process is the classical LMS algorithm [3], given by

$$W_{(n+1)} = W_{(n)} - (\mu/2)\nabla\xi \tag{7}$$

where $(n+1)$ and (n) are the new and previous sample numbers, respectively. μ is the adaptive step size and ∇ is the derivative with respect to the weight adjustment vector W. From equations (4) and (6)

$$\nabla\xi = \nabla \sum_{m=1}^{M} E_m^2 = 2X'E, \qquad X' = \hat{C} * X, \tag{8}$$

giving

$$W_{(n+1)} = W_{(n)} - \mu X'E. \tag{9}$$

X' is known as the 'filtered X' source signal and $\hat{C}$ can be an adequate representation/estimation of C.

2.6. FREQUENCY DOMAIN

In the frequency domain each of the expressions below is a function of frequency, ω (not shown). For a steady discrete primary source, $X = 1$, equations (4), (7) and (8) (see Appendix) give the general frequency domain relationship as

$$E = D + CW, \qquad \xi = E^H E \qquad \nabla\xi = 2C^{\mathrm{H}}E, \tag{10}$$

$$W_{(n+1)} = W_{(n)} - \mu C^{\mathrm{H}}E, \tag{11}$$

or, upon substituting equation (10) back into equation (11)

$$W_{(n+1)} = [I - \mu C^{\mathrm{H}}C]W_{(n)} - \mu C^{\mathrm{H}}D \tag{12}$$

I is a unity diagonal matrix and H is the Hermitian transpose of the complex conjugate of C. Because the total error surface ξ is quadratic (bowl shaped),

differentiation of ξ, with respect to W, equation (8), and equating to zero gives the minimum (bottom of the bowl) value: i.e., optimum W_0 given by

$$W_0 = -(C^{\mathrm{H}}C)^{-1}C^{\mathrm{H}}D. \tag{13}$$

This is the Wiener solution which is equivalent to equation (19), given in reference [1] and is identical to equation (5.3.45), in reference [6]. Substituting back in equations (4) and (6), or equation (19) in equation (18) in reference [1] (see Appendix) gives the minimum total error $\xi_{\min}$ as

$$\xi_{\min} = D^{\mathrm{H}}[I - C(C^{\mathrm{H}}C)^{-1}C^{\mathrm{H}}]D. \tag{14}$$

2.7. PRACTICAL SYSTEM

Figure 5 shows a physical implementation of the schematic control system given in Figure 4. Syn represents the synthesis of the sound X^*, synchronized from the primary source X.

Alternatively a microphone could be used to measure X. Unfortunately a feedback path is then created between the secondary source loudspeaker and this microphone. The arrangement then has the potential to become unstable, requiring various schemes, such as infinite impulse response (IIR) filters, to reduce the instability. The functions H_f, H_c and H_m represents the transfer functions of the signal conditioning filters, cancelling sources and microphones respectively. H_r is the transfer function for the propagation distance between the sources and microphones which is equivalent to a phase retardation.

For a single frequency primary noise signal, the elements of the propagation matrix C can be replaced by simple delays. This modification of the previously described filtered $\times$ LMS algorithm is known as the delayed $\times$ LMS algorithm. It significantly reduces the computation requirements of the ANC system, and provides a simpler characterization of the adaptive process. In the frequency domain, the individual stability regions and the individual components of the complete transfer function of the adaptive process can be isolated and investigated directly. This then allows the quality of the stability performance to be investigated in terms of bandwidth, attenuation depth, speed of convergence and spectral distortion as a function of frequency.

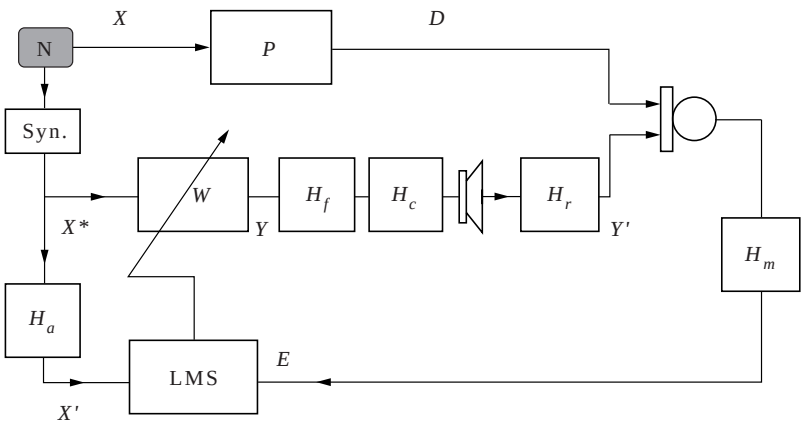

Figure 5. Practical control system.

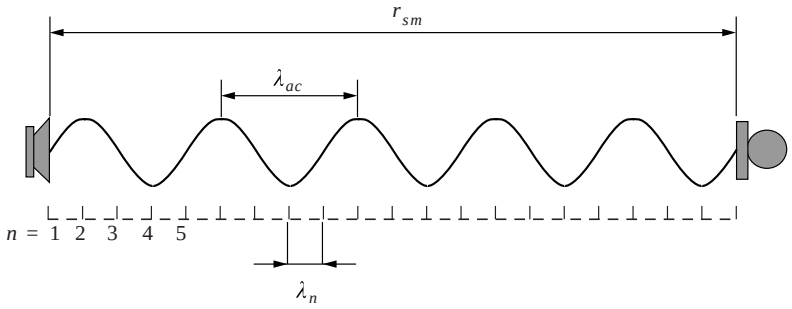

Figure 6. Discrete space.

For a single discrete frequency, W can be adequately implemented as a 2 tap FIR filter. The transfer function around the control loop, $Y - E$ in Figure 5, can then be written as

$$G_{tf} = \frac{Y'}{Y}\frac{E}{Y'} = \frac{E}{Y} = H_f H_c H_m H_r. \tag{15}$$

A further phase term is introduced by the delayed LMS algorithm which effectively introduces a fifth transfer function H_a. This is equivalent to a phase advance making the overall transfer function

$$G_{tf} = H_f H_c H_m H_r H_a. \tag{16}$$

This function can be represented by two terms,

$$G_{tf} = G_{em}\, \mathrm{e}^{\mathrm{j}\omega T} \tag{17}$$

where

$$G_{em} = H_f H_c H_m \qquad \text{and} \qquad T = T_a - T_r - T_{em}. \tag{18}$$

G_{em} represents the amplitude term and T_{em} the delay time of the electromechanical system and T_a and T_r represents the corresponding time advance and retardation times, respectively. Basically the adaptive loop is convergent when the phase angle ($\phi = \omega T$) of equation (17) is equal to an integer number of 2π radians: i.e.,

$$\phi = \angle G_{tf} = 2\pi N \pm \pi/2, \qquad N = 0, 1, 2, \ldots. \tag{19}$$

Thus there are N stability regions occurring at multiples of 2π and of width $\pm\pi/2$ radians where some degree of adaptive convergence can be expected.

2.8. STABILITY (REGION) PREDICTION

Because the physical system is implemented digitally, propagation space and the corresponding equations become discretized.

Figure 6 illustrates the propagation space between a secondary source and microphone, discretized by the sampling time T_n. Here n is the sample number, f_{ac} and λ_{ac} are the acoustic source frequency and wavelength respectively and c_0 is the sound propagation speed (taken to be 340 m/s in the computations). Also f_n

and λ_n are the sampling frequency and sampling length, respectively. The following relations are then self evident:

$$\text{acoustic wavelength,} \qquad \lambda_{ac} = c_0/f_{ac} = T_{ac}c_0; \tag{20}$$

$$\text{sampling period,} \qquad T_n = 1/f_n; \tag{21}$$

$$\text{sampling time,} \qquad T = nT_n; \tag{22}$$

$$\text{sampling length,} \qquad \lambda_n = T_n c_0 = c_0/f_n; \tag{23}$$

$$\text{number of samples in distance } r_{sm} \qquad n_r = r_{sm}/\lambda_n = (r_{sm}/c_0)f_n = t_r/T_n; \tag{24}$$

$$\text{number of samples in distance } \lambda_{ac}, \qquad n_{\lambda_{ac}} = \lambda_{ac}/\lambda_n = (\lambda_{ac}/c_0)f_n = f_n/f_{ac}; \tag{25}$$

$$\text{change in number of samples for a change in } f_{ac} \qquad \Delta n = -(f_n/f_{ac}^2)\Delta f_{ac}; \tag{26}$$

$$\text{change in phase } \phi \text{ for a change in } n, \qquad \Delta\phi = 2\pi f_{ac}\Delta T = (2\pi f_{ac}/f_n)\Delta n. \tag{27}$$

In discrete space the corresponding transfer function from equations (17), (18), (22) becomes

$$G_{tf} = G_{em}\, \mathrm{e}^{\mathrm{j}\omega(n_a - n_r + n_{em})\tau_n} \tag{28}$$

where n_a and n_r are the advance and retarded sample numbers respectively. n_{em} is the equivalent number of samples for the electromechanical transfer function, which is of course a function of acoustic source frequency f_{ac}, thus

$$n_{tf} = n_a - n_r + n_{em} \tag{29}$$

In terms of the number of stability regions (2π radians or wavelengths)

$$N_{tf} = N_a - N_r + N_{em} \tag{30}$$

where the number of equivalent wavelengths in n_a is:

$$N_a = \frac{n_a}{n_{ac}} = n_a \frac{f_{ac}}{f_n} \tag{31}$$

and the number of wavelengths in the distance r_{sm} becomes:

$$N_r = \frac{r_{sm}}{\lambda_{ac}} = r_{sm} \frac{f_{ac}}{c_0} \tag{32}$$

Thus

$$N_{tf} = \left(\frac{n_a}{f_n} - \frac{r_{sm}}{c_0}\right) f_{ac} + N_{em} \tag{33a}$$

and

$$N_{tf} = N_{emr}(n_a = n_r = r_{sm}f_n/c_0) = N_{em}(n_a = n_r = 0) \tag{33b}$$

N_{em} is the electromechanical phase number transfer function of the system alone, i.e. for zero propagation distance between s and m, and N_{emr} is the phase number transfer function modified by reflections between s and m. If the propagation space is anechoic (non-reflecting) then $N_{emr} = N_{em}$. The N_{tf} is important, it allows the stability of the adaptive process to be investigated as a function of the propagation space and environment changes. For good cancellation, it is essential that an accurate knowledge of this transfer function is obtained. This can be found manually, through direct measurement of the stability regions, or automatically through white noise/impulse testing techniques.

Rearranging equation (33) in terms of the sample number and $N_{tf} \to N$ (integer numbers) and $N_{em} \to N_{emr}$ generally for non-anechoic conditions, one has

$$n_a = \left(\frac{N - N_{emr}}{f_{ac}} + \frac{r_{sm}}{c_0} \right) f_n \tag{34}$$

Equation (34), describes the stability regions in the acoustic frequency domain as a function of the adjustable sample number n_a. This is implemented through the delayed LMS algorithm, it can adjust the region's position within the frequency spectrum. Relative to n_r (the wave propagation sample delay), n_a is actually a sample advance term.

The dominant feature of equation (34) occurs when the N contours transform from a vertical to a horizontal direction, as the acoustic frequency goes to infinity (large value). Here, for example

$$(N - N_{emr}) f_n / f_{ac} \approx 10 \qquad \text{giving} \qquad n_a \approx 10 + r_{sm} f_n / c_0 \tag{35}$$

The accuracy of prediction, using the equation (34), will depend on how well N_{emr} is known as a function of frequency. If the propagation space is not anechoic, then the N_{emr} function could be multivalued (having ripples resulting through reflections), then stability region splitting could result for the same N. If $n_a / f_n \gg r_{sm} / c_0$, region splitting will be less obvious through reflections.

2.9. FREE-FIELD SYSTEM ROBUSTNESS

We now investigate the second condition considered necessary for multichannel systems to converge effectively. This is that the transfer function of the multichannel plant has to be robustly stable [5, 6]. In our application the dominant plant is the free-field propagation matrix between the secondary sources and microphones. The robustness of this free-field system is established by using, firstly, conventional condition methods, and secondly, a novel sum and difference acoustic theory. For simplicity a two channel system is used initially to demonstrate the basic properties. Higher channel numbers (4 and 6) are then considered.

2.10. PROPAGATION MATRIX

Consider the sound pressures P_1 and P_2 at microphones positions 1 and 2 from secondary (cancelling) sources of strength Q_1 and Q_2, as illustrated in Figure 7.

$$P_1 = C_{11} Q_1 + C_{12} Q_2, \qquad P_2 = C_{21} Q_2 + C_{22} Q_2. \tag{36, 37}$$

C_{sm} are the propagation elements between the secondary sources (cancellers) s and microphones m given by

$$C_{sm} = R_{sm}\, e^{jkr_{sm}}, \tag{38}$$

where $k = 2\pi/\lambda = \omega/c_0$ is the wave number, (39a)

$R_{sm} = \omega\rho_0/4\pi r_{sm}$ is the amplitude term. (39a)

In the above relations r_{sm} is the source/microphone distance, λ is the acoustic wavelength, c_0 is the speed of sound, ω is the frequency and ρ_0 is the propagation medium density. The source strength Q, which can be represented, for example, by a small sphere of radius a and surface velocity u, is defined by the relation

$$Q = u4\pi a^2. \tag{40}$$

Equations (36) and (37) are now written in matrix form as

$$\begin{bmatrix} P_1 \\ P_2 \end{bmatrix} = \begin{bmatrix} C_{11} & C_{12} \\ C_{21} & C_{22} \end{bmatrix} \cdot \begin{bmatrix} Q_1 \\ Q_2 \end{bmatrix}. \tag{41}$$

Here, $[C_{sm}]$ is the propagation matrix in free space; it is the transfer function between the input Q_1, Q_2 and the output P_1, P_2. Its elements can be expressed in the complex form, where, from equations (38, 39)

$$C_{sm} = a_{sm} + jb_{sm}, \qquad a_{sm} = R_{sm} \cos kr_{sm}, \qquad b_{sm} = R_{sm} \sin kr_{sm}. \tag{42}$$

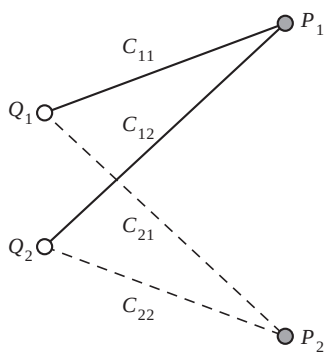

Figure 7. Free field propagation space.

2.11. EIGENVALUES

Eigenvalues, which are the roots of the characteristic equation of the transfer function, determine the robustness of the system. In this case, depending on how close the values are to the imaginary axis on the right hand side of the s plane, or how close to the inside of the unit circle, in the z plane. They are obtained from the propagation matrix equation through

$$\det [\varepsilon I - C_{sm}^{\mathrm{H}} C_{sm}] = 0, \tag{43}$$

where ε is the eigenvalue, I is the unit matrix of appropriate order,

$$I = \begin{bmatrix} 1 & 0 \\ 0 & 1 \end{bmatrix},$$

and H denotes the transpose of the complex conjugate.

Using general complex numbers and matrix notation shows that if

$$C = \begin{bmatrix} a_{11} + \mathrm{j}b_{11} & a_{12} + \mathrm{j}b_{12} \\ a_{21} + \mathrm{j}b_{21} & a_{22} + \mathrm{j}b_{22} \end{bmatrix} \qquad C^{\mathrm{H}} = \begin{bmatrix} a_{11} - \mathrm{j}b_{11} & a_{21} - \mathrm{j}b_{21} \\ a_{12} - \mathrm{j}b_{12} & a_{22} - \mathrm{j}b_{22} \end{bmatrix}, \tag{44}$$

then

$$C^{\mathrm{H}}C = \begin{bmatrix} (a_{11} + \mathrm{j}b_{11})(a_{11} - \mathrm{j}b_{11}) + (a_{12} + \mathrm{j}b_{12})(a_{12} - \mathrm{j}b_{12}) & (a_{11} + \mathrm{j}b_{11})(a_{21} - \mathrm{j}b_{21}) + (a_{12} + \mathrm{j}b_{12})(a_{22} - \mathrm{j}b_{22}) \\ (a_{21} + \mathrm{j}b_{21})(a_{11} - \mathrm{j}b_{11}) + (a_{22} + \mathrm{j}b_{22})(a_{12} - \mathrm{j}b_{12}) & (a_{21} + \mathrm{j}b_{21})(a_{21} - \mathrm{j}b_{21}) + (a_{22} + \mathrm{j}b_{22})(a_{22} - \mathrm{j}b_{22}) \end{bmatrix}, \tag{45}$$

giving

$$C^{\mathrm{H}}C = \begin{bmatrix} f_{11} & g_{12} \\ g_{21} & f_{22} \end{bmatrix}, \tag{46}$$

where

$$\begin{aligned} f_{11} &= a_{11}^2 + b_{11}^2 + a_{21}^2 + b_{21}^2, \\ g_{12} &= a_{11}a_{12} + b_{11}b_{12} + a_{21}a_{22} + b_{21}b_{22} - \mathrm{j}a_{11}b_{12} + \mathrm{j}a_{12}b_{11} - \mathrm{j}a_{21}b_{22} + \mathrm{j}a_{22}b_{21}, \\ g_{21} &= a_{12}a_{11} + b_{12}b_{11} + a_{22}a_{21} + b_{22}b_{12} - \mathrm{j}a_{12}b_{11} + \mathrm{j}a_{11}b_{12} - \mathrm{j}a_{22}b_{21} + \mathrm{j}a_{21}b_{22}, \\ f_{22} &= a_{12}^2 + b_{12}^2 + a_{22}^2 + b_{22}^2. \end{aligned} \tag{47}$$

Generally, for a symmetrical matrix, suffices 11 = 22 and 12 = 21, equation (43) becomes

$$\det \left[\begin{bmatrix} \varepsilon & 0 \\ 0 & \varepsilon \end{bmatrix} - \begin{bmatrix} f & g \\ g & f \end{bmatrix} \right] = \det \begin{bmatrix} \varepsilon - f & -g \\ -g & \varepsilon - f \end{bmatrix} = (\varepsilon - f)^2 - g^2, \tag{48}$$

and equating to zero one has

$$\varepsilon^2 - 2f\varepsilon + f^2 - g^2 = 0. \tag{49}$$

The eigenvalues are then the roots of the above characteristic equation: i.e.,

$$\varepsilon = \frac{2f \pm \sqrt{4f^2 - 4(f^2 - g^2)}}{2} = f \pm g. \tag{50}$$

Thus one can conclude that the eigenvalues are the sums and differences between the diagonal and corner values of the propagation matrix given by

$$\varepsilon = a_{11}^2 + b_{11}^2 + a_{12}^2 + b_{12}^2 \pm 2(a_{11}a_{12} + b_{11}b_{12}), \tag{51}$$

or

$$\varepsilon = R_{11}^2 + R_{12}^2 \pm 2\tilde{R}^2, \tag{52}$$

where, from equation (42),

$$R_{sm} = \sqrt{a_{sm}^2 + b_{sm}^2} \qquad \text{and} \qquad a_{sm} = R_{sm}\cos kr_{sm}, \quad b_{sm} = R_{sm}\sin kr_{sm}, \tag{53a}$$

and

$$\tilde{R} = \sqrt{a_{11}a_{12} + b_{11}b_{12}} = (R_{11}R_{12}\cos \Delta\theta)^{1/2}, \qquad \text{where} \qquad \Delta\theta = k(r_{12} - r_{11}). \tag{53b}$$

$\tilde{R}$ is a mean of R_{11} and R_{12}. Further, if $R_{11} \cong R_{12} \cong R$, then

$$\varepsilon \cong 2R^2 \pm 2R^2 \cong 4R^2 \qquad \text{and} \qquad 0. \tag{54}$$

In general, the characteristic eigenvalues for an arbitrary ECAS geometry are given by equation (43). For a two channel system, the eigenvalues are given by equations (43), (46) and (47). For a symmetrical system, the eigenvalues are given by equations (50), (52) and (53).

2.12. CONDITION NUMBER

As $R \propto 1/r_{sm}$ in equation (54), and if the propagation distances r_{sm} are similar, then the maximum eigenvalue is large and the minimum value small (close to the unstable region in the complex s plane) indicating marginal stability.

Now as the number of channels increases, the number of eigenvalues increases, according to the square of the channel number. This translates into an ever increasing spread of eigenvalues and therefore mode decay rates. The speed of convergence of the fastest mode decay rate will then determine the maximum convergence step size that can be used in the adaptive algorithm, without instability. The bigger ε_{max} the smaller μ_{max}, whereas the minimum eigenvalue will determine the slowest mode decay rate and therefore the largest time constant τ_{max} of the overall system. Thus

$$\mu_{max} \approx 1/\varepsilon_{max} \qquad \text{and} \qquad \tau_{max} \approx T_n/\mu_{max}\varepsilon_{min} \approx T_n K, \tag{55}$$

where

$$K = \varepsilon_{max}/\varepsilon_{min}. \tag{56}$$

T_n is the sampling time and K is the condition number which gives a numerical measure of the robustness of the system. For fast convergence (high robustness,

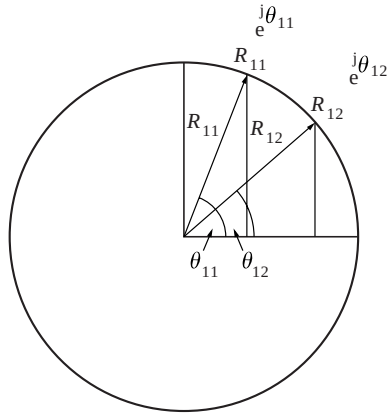

Figure 8. Vectorial addition of two sound pressures.

low K), from equations (40) and (52), the propagation distances r_{sm} need to be as dissimilar as possible.

2.13. ACOUSTIC ROBUSTNESS

An interesting and apparently novel non-matrix method of investigating the robustness of multichannel adaptive systems is to consider the vectorial sum and difference sound pressures, as illustrated in Figure 8, at a microphone from the cancelling sources as shown in Figure 9.

Here

$$P_{11} = R_{11} Q_1 \, e^{j\theta_{11}}, \qquad R_{11} = \omega\rho_0/4\pi r_{11}, \qquad \theta_{11} = kr_{11}, \tag{57}$$

$$P_{12} = R_{12} Q_2 \, e^{j\theta_{12}}, \qquad R_{12} = \omega\rho_0/4\pi r_{12}, \qquad \theta_{12} = kr_{12}, \tag{58}$$

where the quantities are defined in equations (38)–(40).

The sum and difference pressure, per unit source strength Q (upon assuming $Q_1 = Q_2$) then becomes

$$P_{\pm}/Q = R_{11} \, e^{j\theta_{11}} \pm R_{12} \, e^{j\theta_{12}} = R_{11}(\cos\theta_{11} + j \sin\theta_{11}) \pm R_{12}(\cos\theta_{12} + j \sin\theta_{12})$$

$$= R_{11} \cos\theta_{11} \pm R_{12} \cos\theta_{12} + j(R_{11} \sin\theta_{11} \pm R_{12} \sin\theta_{12}). \tag{59}$$

Taking the modulus and squaring the above equation gives

$$|P_{\pm}/Q|^2 = (R_{11} \cos\theta_{11} \pm R_{12} \cos\theta_{12})^2 + (R_{11} \sin\theta_{11} \pm R_{12} \sin\theta_{12})^2$$

$$= R_{11}^2 \cos^2\theta_{11} \pm 2R_{11}R_{12} \cos\theta_{11} \cos\theta_{12} + R_{12}^2 \cos^2\theta_{12} + R_{11}^2 \sin^2\theta_{11}$$

$$\pm 2R_{11}R_{12} \sin\theta_{11} \sin\theta_{12} + R_{12}^2 \sin^2\theta_{12}, \tag{60}$$

which reduces to

$$\varepsilon = |P_{\pm}/Q|^2 = R_{11}^2 + R_{12}^2 \pm 2R_{11}R_{12}\cos \Delta\theta, \qquad \text{where} \qquad \Delta\theta = \theta_{11} - \theta_{12}. \quad (61)$$

Equation (61) is equivalent to equation (52); it therefore determines also the eigenvalues of the system. Its physical meaning is interpreted below.

2.14. PHASE DIFFERENCE

The phase difference $\Delta\theta = \theta_{11} - \theta_{12}$ in equation (61) is related to the path difference Δr between each source and the microphone (in the far field), given by

$$\Delta\theta = k\Delta r, \qquad k = 2\pi/\lambda, \qquad \Delta r \cong r_{12} - r_{11}. \quad (62)$$

From the free-field geometry shown in Figure 9, where now a, b and c have the meaning illustrated in that figure, it is obvious that

$$r_{11} = \sqrt{c^2 + \left(\frac{b-a}{2}\right)^2} = c\left[1 + \left(\frac{b-a}{2c}\right)^2\right]^{\frac{1}{2}} \cong c\left[1 + \frac{1}{2}\left(\frac{b-a}{2c}\right)^2\right] \quad (63)$$

$$\text{and } r_{12} = \sqrt{c^2 + \left(\frac{b+a}{2}\right)^2} = c\left[1 + \left(\frac{b+a}{2c}\right)^2\right]^{\frac{1}{2}} \cong c\left[1 + \frac{1}{2}\left(\frac{b+a}{2c}\right)^2\right], \quad (64)$$

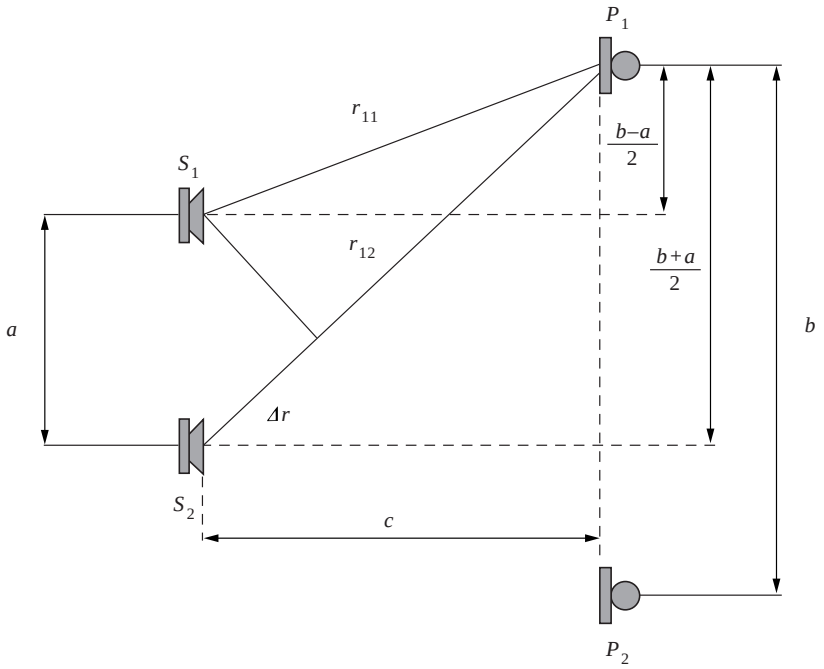

Figure 9. ECAS geometry.

providing

$$c \gg b + a. \tag{65}$$

Thus the path difference can be expressed as

$$\Delta r \cong r_{12} - r_{11} \cong c\left(\left(1 + \frac{1}{2}\left(\frac{b+a}{2c}\right)^2\right) - \left(1 + \frac{1}{2}\left(\frac{b-a}{2c}\right)^2\right)\right), \tag{66}$$

$$\text{or simply } \Delta r \cong \frac{(b+a)^2 - (b-a)^2}{8c} = \frac{ab}{2c}. \tag{67}$$

Finally, the phase difference in equation (62) then becomes simply

$$\Delta\theta \cong \pi ab/\lambda c. \tag{68}$$

2.15. SUM AND DIFFERENCE SPECTRA

One can now return to the sum and difference equation (61): i.e.,

$$\varepsilon = |P_{\pm}/Q|^2 = R_{11}^2 + R_{12}^2 \pm 2R_{11}R_{12}\cos\Delta\theta.$$

The sum (ε_+) and difference (ε_-) eigenvalues have alternative coincident maxima and minima when

$$|\cos\Delta\theta| = 1, \qquad \text{i.e., when} \qquad \Delta\theta = \theta_{11} - \theta_{12} = m\pi, \qquad \text{where}$$

$$m = 0, 1, 2, 3, \ldots, \tag{69}$$

or, from equation (62), when

$$\Delta r = \Delta\theta/k = m(\lambda/2): \tag{70}$$

i.e., when Δr is equal to a multiple of half wavelengths.

The maxima and minima of $|P_+/Q|^2$ then become

$$\varepsilon = |P_{\pm}/Q|^2 = R_{11}^2 + R_{12}^2 \pm 2R_{11}R_{12}, \qquad \text{or} \qquad \varepsilon = (R_{11} \pm R_{12})^2. \tag{71}$$

And from equations (56) and (39) the value of the condition number is given by

$$K = \varepsilon_{max}/\varepsilon_{min} = [(R_{11} + R_{12})/(R_{11} - R_{12})]^2 = [(r_{12}/r_{11} + 1)/(r_{12}/r_{11} - 1)]^2, \tag{72}$$

which can become large. In fact if $R_{11} \cong R_{12} \cong R$ then

$$\varepsilon = |P_{\pm}/Q|^2 \approx 4R^2, \qquad \text{or} \qquad 0, \qquad \text{and} \qquad K \approx \infty, \tag{73}$$

which is identical to equation (54).

Finally, the positions of the peaks in the condition number can be found in the frequency domain from equations (68) and (69): i.e.,

$$\Delta\theta = m\pi = \pi ab/\lambda c, \qquad \text{giving} \qquad \lambda = ab/m, \tag{74}$$

giving

$$f_m = c_0/\lambda = mc_0(c/ab), \qquad \text{where } m = 0, 1, 2, 3, \ldots. \tag{75}$$

For $c \gg (b + a)$, in Figure 9, equation (72) can be used to estimate the maximum values in the condition spectra, and equation (75) their positions. Equation (70) predicts that these maxima occur at multiples of $\lambda/2$. Amazingly, even with a large number of propagation paths, as in large channel number systems, equation (75) can still basically hold, providing a is replaced by the source spacing d, given by

$$d = D/(N_s - 1), \tag{76}$$

where D is the source dimension and N_s is the number of equispaced sources along the dimension.

2.16. MATRIX CONDITION SPECTRA

Figure 10 gives details of the system condition spectra. The geometry is for a two channel ECAS system as shown in Figure 9, where $a = 2$ m, $b = 5$ m and $c = 10$ m. Figure 10(a) shows the diagonal and corner values of the $C^{H}C$ matrix in equation (43), with frequency. Figure 10(b) shows the inverse of the difference between the diagonal and corner values showing high periodic values when the corner values approach the diagonal values. Figure 10(c) shows the matrix eigenvalues as a series of maxima and minimum, increasing with frequency.

Figure 10(d) shows the matrix condition number (ratio of the maximum to minimum eigenvalues). It can now be seen that the characteristic free-field matrix condition spectra is comb shaped. The condition number is very low over most of the spectrum. However, large values occur at (a) very low frequency where the propagation path differences in terms of the acoustic wavelength are small, and (b) periodic points within the spectrum, given by equation (75). High condition numbers need to be avoided if the adaptive process is to converge.

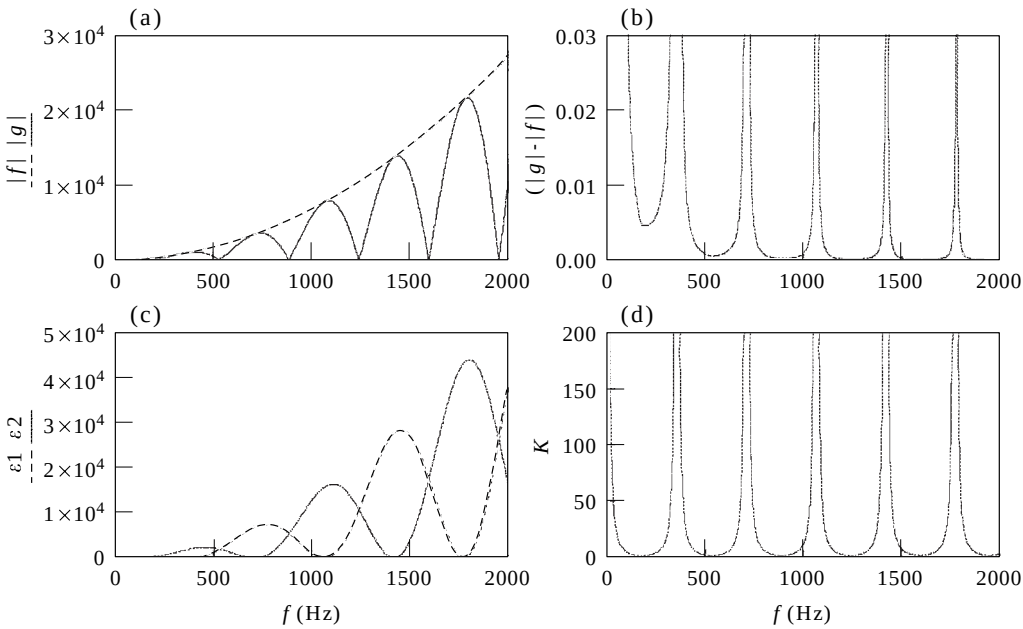

Figure 10. Characteristic of free-field matrix condition spectra (2 × 2 matrix). (a) Diagonal and corner elements of $C^{H}C$ matrix; (b) inverted difference between diagonal and corner elements; (c) eigenvalues; (d) condition number: max (ε_1 or ε_2)/min (ε_1 or ε_2).

2.17. SUM AND DIFFERENCE SPECTRA

Figure 11 gives details of the sum and difference acoustic spectra. Again the geometry is for a two channel ECAS system as shown in Figure 9, with the same dimensions as in the previous section. Figures 11(a) and (b) show the magnitude R_{sm} and phase difference kr_{sm} between the two propagation elements C_{11} and C_{12}, where

$$\text{propagation elements,} \quad C_{11} = (\omega\rho/4\pi r_{11})\, e^{jkr_{11}}, \qquad C_{12} = (\omega\rho/4\pi r_{12})\, e^{jkr_{12}};$$

$$\text{sum and difference,} \quad S = C_{11} + C_{12}, \qquad D = C_{11} - C_{12}.$$

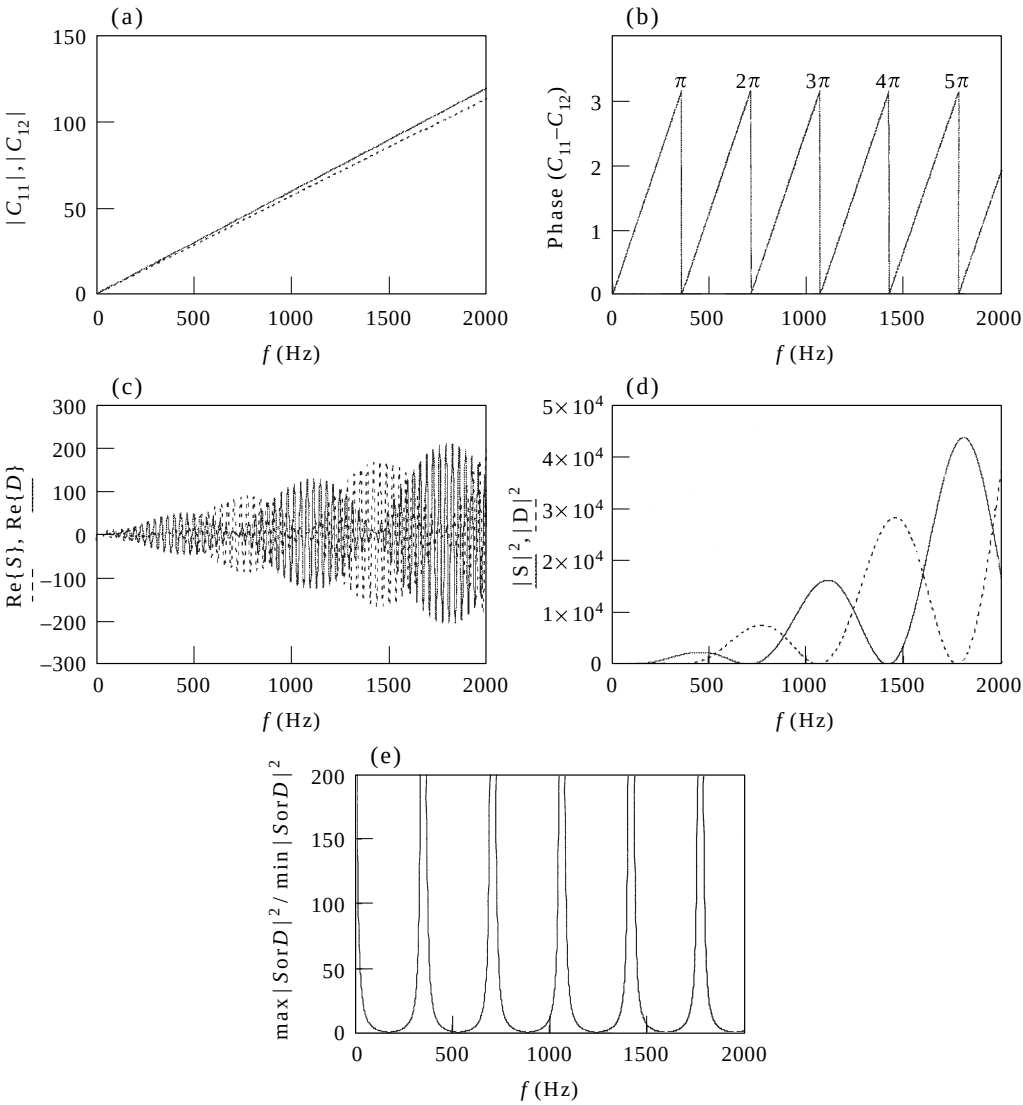

Figure 11. Details of the sum and difference spectra (2×2 matrix). Propagation elements: $C_{11} = (\omega\rho/4\pi r_{11})\, e^{jkr_{11}}$; $C_{12} = (\omega\rho/4\pi r_{12})\, e^{jkr_{12}}$; also $S = C_{11} + C_{12}$, $D = C_{11} - C_{12}$. (a) Magnitudes; (b) phase; (c) real parts of S and D; (d) squared magnitudes of S and D; (e) max/min ratios.

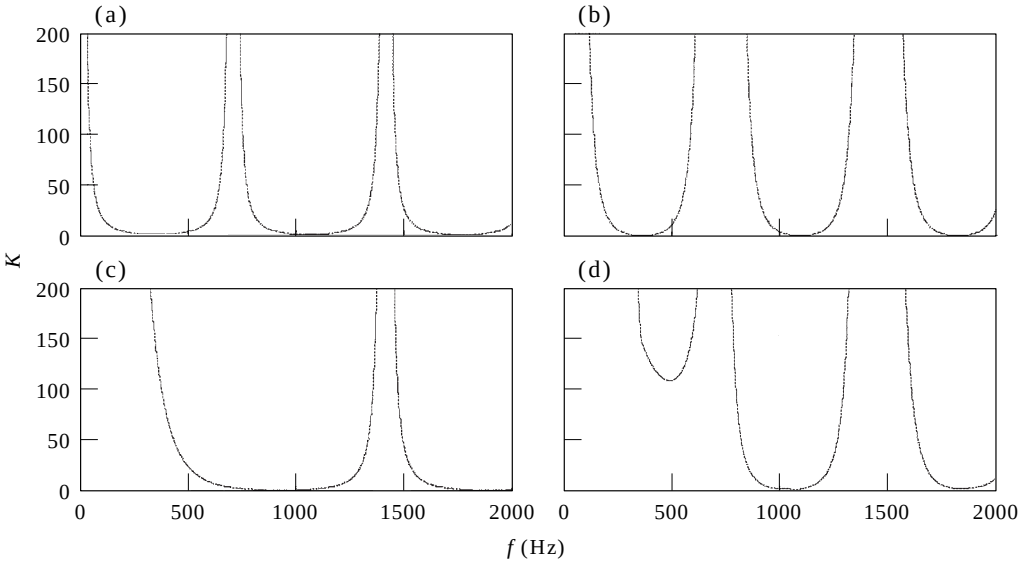

Figure 12. Multichannel system condition spectra. Channel system: (a) 1×2; (b) 2×2; (c) 1×3; (d) 2×3.

The magnitude differences gradually increase with frequency whereas the phase differences rapidly increase (shown in step size of π radians). Figure 11(c) shows the real part of the sum and difference of the propagation elements C_{11} and C_{12}. The modulation amplitude increases with frequency, the maxima of one function coinciding with zeros in the other. Note that successive zeros, given by alternate functions, are given by equation (75). Figure 11(d) shows the sum and difference function magnitude squared given by equation (61). Figure 11(e) shows the ratio of the maximum to minimum squared values of the sum and difference functions. It can be seen that the matrix condition spectra in Figure 10, and the sum and difference acoustic spectra in Figure 11 are equivalent.

Thus it can be seen that maxima in the condition spectra occur when the path difference between the sources and detectors corresponds to multiples of half wavelengths or phase differences of π radians.

2.18. MULTICHANNEL CONDITION SPECTRA

Figure 12 shows the multichannel condition spectra for 2 and 4 channels (2 layers of 2, separated by 1 m), and 3 and 6 channels (2 layers of 3, separated by 1 m) for ECAS system dimensions $a = 1$ m, $b = 5$ m and $c = 10$ m. Again the half wavelength spectral peaks, even for moderate channel numbers, are basically given by equation (75). Also that the peaks thicken (overall condition deteriorates) as the channel number increases.

These spectra are for simple symmetrical geometries. The spectral peaks can be manipulated if need be by customizing the ECAS geometry.

3. MEASURED DATA

After the preceding consideration of the hardware and the control strategy for the system to adapt effectively, the resulting data is now discussed.

3.1. MEASURED STABILITY REGIONS

Figure 13 shows the measured stability regions of equation (34) measured for a single channel plotted as a function of acoustic source frequency f_{ac}, sample advance number n_a, and for a secondary source—microphone propagation distance of $r_{sm} = 0{\cdot}12$ m (speaker close to microphone). From equation (24) and a sample frequency of $f_n = 4000$ Hz, this distance corresponds to a sample retardation number of $n_r = 1{\cdot}4$. The phase contours of N multiples of exactly 2π radians are also shown. This figure illustrates that there are N stability regions for any sample advance number n_a. Or conversely, for any one frequency f_{ac} and propagation distance r_{sm} (n_r number), there is an almost infinite number of stability regions that can be selected by adjusting n_a. The main feature of Figure 13, situated at $n_a \approx 12$, as $f_{ac} \to \infty$ is given approximately by equation (35). N_{em} as a function of N can be found when $n_a = 0$.

3.2. MEASURED TRANSFER FUNCTION

Figure 14 shows the same data replotted in terms of the more familiar phase angle ϕ versus acoustic source frequency f_{ac}, for various sample advance numbers n_a. The N stability regions are now indicated by the horizontal shaded bars of width π radians.

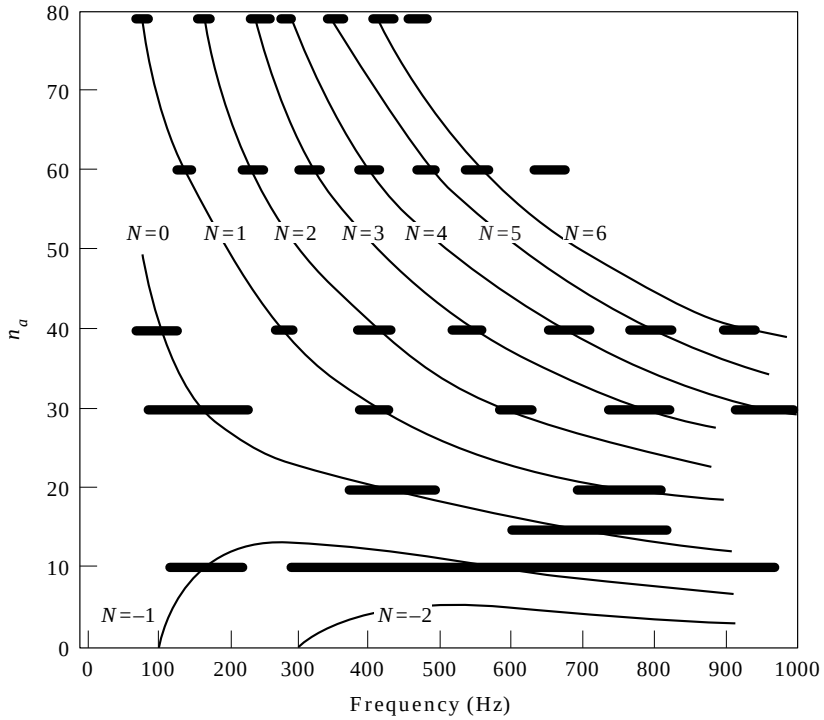

Figure 13. Measured stability regions; $r_{sm} = 0{\cdot}12$ m ($n_r = 1{\cdot}4$).

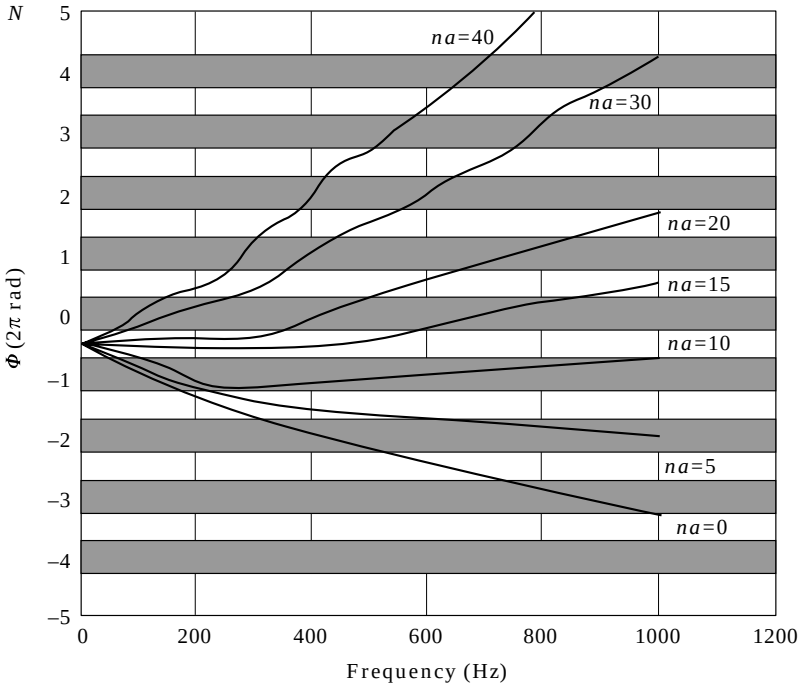

Figure 14. Measured transfer functions; $r_{sm} = 0{\cdot}12$ m ($n_r = 1{\cdot}4$).

The phase part of the transfer function (Bode diagram), of the electromechanical system is obtained when the speaker and microphone are in contact, i.e. when $n_a = n_r = 0$; then $n_{tf} = n_{em}$, $N_{tf} = N_{em}$ in equations (29), (30) and (33). The closest distance measured is for $r_{sm} = 0{\cdot}12$ m, i.e. $n_a = n_r = 1{\cdot}4$, as given in Table 1. The closest curve shown in Figure 14 is for $n_a = 0$. The $-\pi$ or $(-N/2)$, at zero frequency, is implemented by the FIR filter.

It can be seen now that G_{tf} in equations (17), (18) or (28), can be represented approximately by a multipole filter of the form

$$G_{tf} = 1/(1 + j\omega\tau_e)^p, \qquad (r_{sm} = 0) \tag{35}$$

where τ_e is the effective time constant and p is the equivalent multipole order. From Table 1 and extrapolation over a frequency range of 10 kHz, $\angle G \cong 7\pi$, $p \cong 14$. The "corner" frequency ($\omega \cong 1/\tau_e$) having a phase of $3{\cdot}5\ \pi$ at $f_{ac} \approx 440$ Hz gives $\tau_e = (2\pi f_{ac})^{-1} = 0{\cdot}36$ ms.

Figure 15 shows similar measured stability regions for a propagation distance of $r_{sm} = 3$ m ($n_r = 35{\cdot}3$). Apart from changes in N_{tf}, Figures 13 and 15 are

TABLE 1

Electromechanical transfer function (phase) of the adaptive system; $n_a = n_r = 1{\cdot}4$

$-N_{tf}$	0·5	0·99	1·45	1·83	2·14	2·39	2·59	2·75	2·88	2·99	3·07
f_{ac}	0	100	200	300	400	500	600	700	800	900	1000

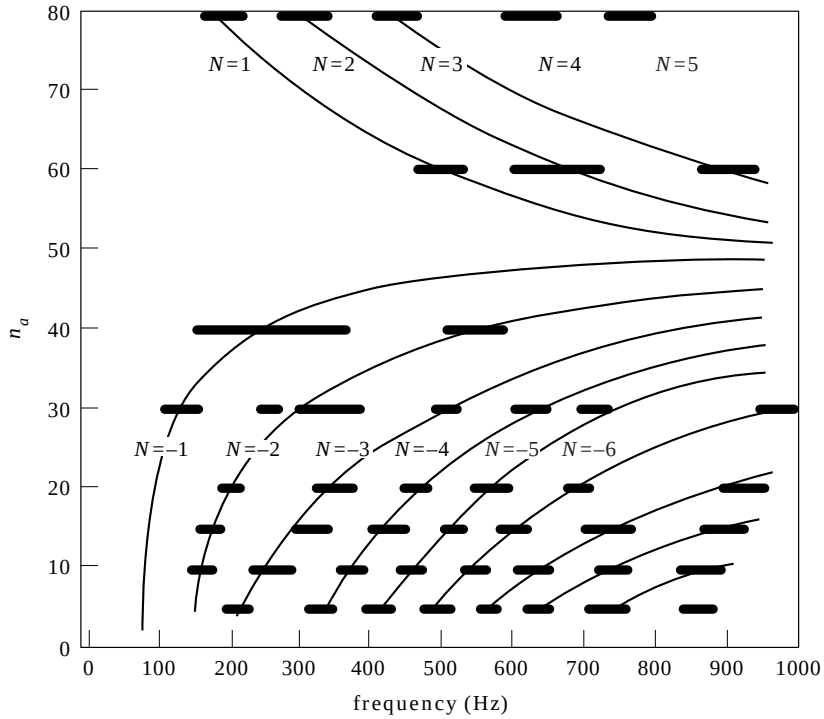

Figure 15. Measured stability regions; $r_{sm} = 3$ m ($n_r = 35{\cdot}3$).

equivalent when plotted in terms of n_{tf}, where, from equation (29), $n_{tf} = n_a - n_r + n_{em}$. Thus Figure 15 can be converted approximately to Figure 13 by subtracting the equivalent n, corresponding to the difference in propagation distances: i.e., $3\text{ m} - 0{\cdot}12\text{ m} \equiv 35{\cdot}3 - 1{\cdot}4 \approx 34n$. The other differences between Figures 14 and 15 occur through the modification of N_{tf}, by reflection from the hard floor, which in this case was left purposely untreated. The main changes occur around $n_a = 30$, with region splitting at about $f_{ac} = 300$ Hz and region displacement at about 800 Hz. The modified transfer function N_{emr}, including effects of reflection, is found from Figure 15, equation (33), when $n_a = n_r = 35{\cdot}3$. The dominant feature at $n_a \approx 48$, as $f_{ac} \to \infty$, is given approximately by equation (35). Further theoretical information on stability criteria can be found in references [7–9].

3.3. STABILITY REGION ALIGNMENT

For each channel number N_c there will be N_c^2 propagation paths r_{sm}, and therefore $N_c^2 N$ spectrum stability regions to investigate. To demonstrate the concept, a two channel system is used, Figure 16 shows the spectrum stability strips for this system. The channels are labelled 2 and 7 for both sources and microphones, at a nominal source-microphone propagation distances of $r_{sm} = 1{\cdot}5$ m; see Figure 2 for ECAS details. Also given are the first four stability regions $N = -1$ to -4. These have been approximately measured and aligned, by adjusting the phase advance n_a to take into account the difference in each propagation path (direct paths 2-2, 7-7, $n_a = 11$ and cross paths 2-7, 7-2, $n_a = 17$). From equation (24) $n_r \approx 17{\cdot}6$ for $r_{sm} = 1{\cdot}5$ m and $f_n = 4000$ Hz.

Note that all regions are not identical even for the same N. Also some of the regions show splitting, corresponding to ripples in the transfer function allowing the curve to go into and out of the stability regions. The approximate combined measured stability regions are also shown for the 2 channel system. Note that all channel regions have to be aligned at any given frequency for the multichannel adaptation process to converge. This can be accommodated by lateral fine tuning of individual stability regions by adjusting the corresponding n_a.

3.4. STABILITY QUALITY

From equation (19), the nominal stability region length is π radians. However in practice it is found that the region lengths can be a fraction of π, depending primarily on the adaptive step size μ. Typically the range of μ used in these data is 0·01 to 0·1. The maximum value of μ used within each region was found to depend on the source frequency f_{ac} (region stability number N) and position within the region. The maximum stability, and therefore maximum μ used, is not necessarily in the centre of the region (asymmetric region stability). However, towards the edges of the regions, one usually finds that the adaptive performance is considerably degraded. This is usually in terms of lower convergence rate, poorer cancellation and increased harmonic distortion (generation of side bands of the primary source frequency).

To obtain deep shadows within these stability regions, care is needed in optimizing the adaptive process. For example, when using the particular laboratory set-up, the following operating procedures were found.

(1) With high levels of gain (10^4) at the input, 50 Hz electrical "pick up" (odd harmonics only of 50 Hz) is possible in high EM field environments, masking low frequency signals. Solution—good shielding and common mode rejection used at the output from the microphones.

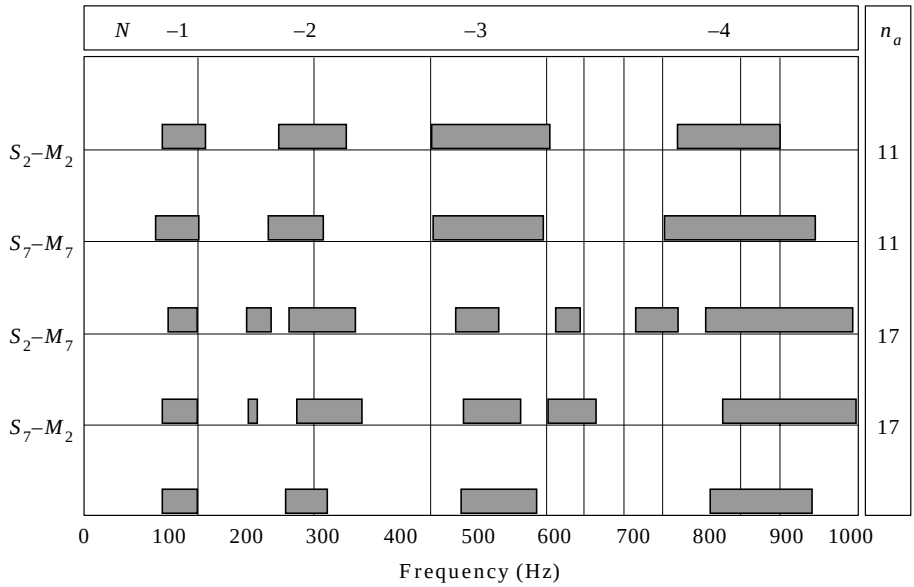

Figure 16. Stability regions for 2 channel ANC system; $r_{sm} = 1{\cdot}5$ m ($n_r = 17{\cdot}6$).

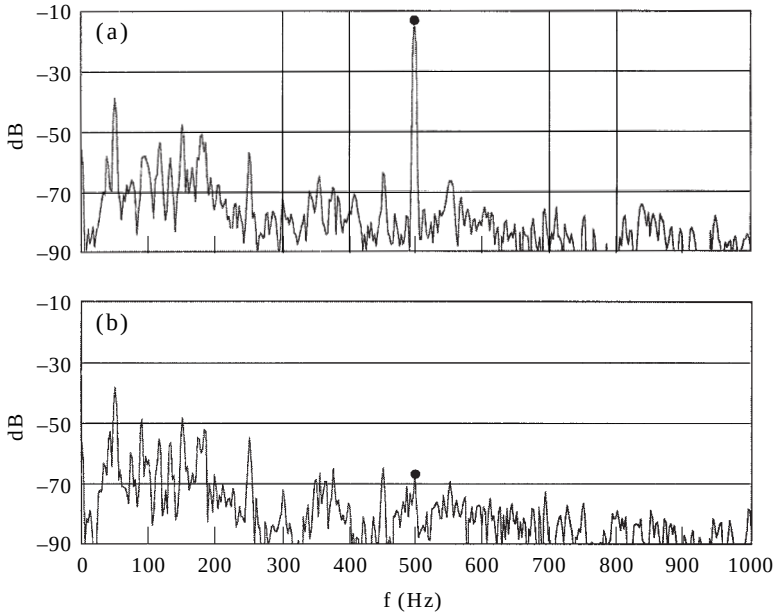

Figure 17. Good cancellation performance. (a) Uncancelled (primary) field in noise, $f = 498$ Hz and $SL = -13{\cdot}6$ dB; (b) cancelled (primary + secondary) field, $SL = -67{\cdot}3$ dB.

(2) Harmonics of the source frequency can easily be generated through overloading the cancelling secondary sources, particularly at low frequencies. Even with moderate levels, harmonics can still be generated through speaker support structure vibration. Solution—dampen structure (in this application hollow support tubes were filled with sand).

(3) As the step μ is increased (faster convergence) the stability bandwidth reduces. As the reference frequency is increased, the filtered x signal (reference oscillator signal amplitude), needs to be increased for maximum attenuation.

(4) At the edge of the stability bands, the adaptive speed reduces. Here, if the reference amplitude x is too big, particularly at low frequencies, harmonics of the reference frequency are generated. If μ and x are too big, side bands of the reference frequency, are generated.

With the above operating guidelines, deep shadows were obtained. Figure 17 is an example of good stability performance. ($r_{sm} = 1{\cdot}5$ m, $f_{ac} = 498$ Hz, $s = 8$, $m = 8$, $n_a = 11$, $N = -3$, $\mu = 0{\cdot}01$). It can be seen that the primary field is completely eliminated, disappearing into the background noise floor of the chamber. The chamber ambient noise at these low frequencies is usually generated by barometric (wind) variations. Odd harmonics of 50 Hz generated by electrical pickup can just about be resolved. The maximum observable attenuation measured with low ambient background noise is about 60 dB. The dynamic range of the electrical equipment (amplifiers) is about 70 dB.

Assuming a properly operated system, we conclude that for optimum convergence rate (highest μ), largest cancellation depth and minimum harmonic distortion, the phase angle around the loop should be close to an exact multiple of 2π radians (approximately in the centre of each region).

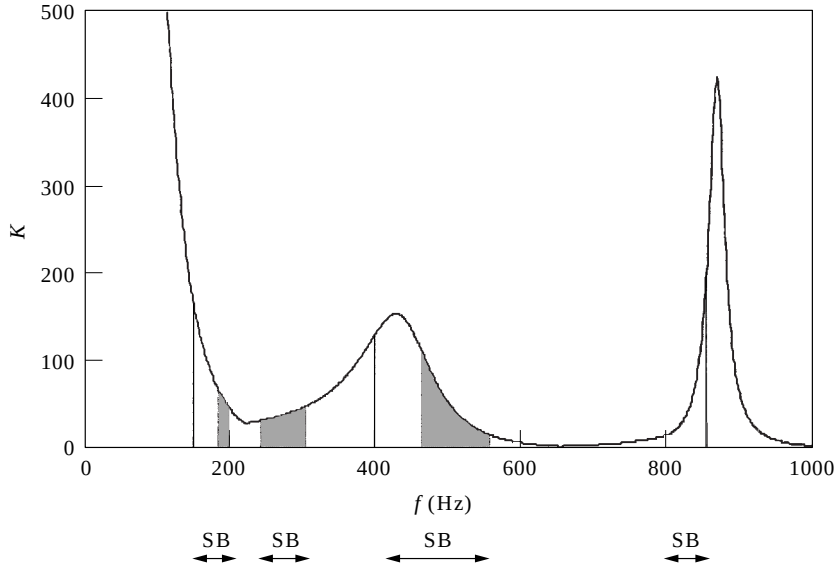

Figure 18. 4 channel ECAS condition spectra; $a = 0{\cdot}98$ m, $b = 1{\cdot}4$ m; $c = 1{\cdot}48$ m.

3.5. MULTI-CHANNEL DATA

For example, in the case of an eight channel system, sixty four propagation paths, each with their own stability regions would have to be considered with some form of automatic region alignment implemented. For simplicity, a four channel system is used to demonstrate the adaptive performance. Details of the laboratory system are illustrated in Figure 2. The dimensions used in taking the following data are shown in Figure 9; they are $a = 0{\cdot}98$ m, $b = 1{\cdot}4$ m, $c = 1{\cdot}48$ m. Figure 18 shows the calculated conditioning spectra according to equations (43) and (56) for a four channel system.

The stability bands for each of the 16 propagation distances between 4 microphones and 4 loudspeakers are aligned at the desired frequency, as described earlier in the text; see Figure 16, for example. The combined (overlapping) stability bands are shown at four different centre frequencies within the spectrum. The shaded regions indicate where the system converges quickly. It can be seen that convergence is easily obtained for condition numbers less than 100.

Within the central part of the stability bands the cancellation is very high at each of the four microphones. The primary sound is completely suppressed into the ambient noise of the chamber giving shadows at the microphones greater than 60 dB, similar to those shown in Figure 17. Values of μ used were from $0{\cdot}001$ giving virtually no convergence, to $0{\cdot}1$ where almost instantaneous convergence was obtained. The leaky LMS algorithm [5], which effectively increases the eigenvalues, artificially reducing the condition number and thus helping non-robust systems to converge (but deteriorates shadow performance), was not used.

4. CONCLUSIONS

A free-field, active noise control theory for the generation of electronically controlled acoustic shadows has been successfully implemented into an adaptive

control system in a purpose built acoustic facility. It is found that two operating conditions are essential for good cancellation performance: (a) complying with control loop stability criteria and (b) operating within multichannel system conditioning robustness.

It is found that for a monochromatic primary source deep shadows at the error detectors greater than 60 dB are obtained, limited only by the ambient sound of the laboratory, provided one observes the following: (a) good system design (linear, large dynamic range hardware); (b) each adaptive loop is operated close to the centre of its stability region; (c) all stability regions are aligned at the frequency of interest (within multiples of 2π radians); (d) the adaptive system is operated within the valleys of its condition spectra; (e) propagation matrix having a condition number greater than 100 should be avoided for practical convergence.

If the above operating conditions, or equivalent, are not implemented, it is unlikely that anything approaching optimum cancellation performance will be achieved.

This paper has demonstrated that deep acoustic shadows can be generated not only in theory but also in practice, providing the adaptive system is properly designed and operated. The concept has been validated for discrete frequencies, laying the foundation for the cancellation of more complex acoustic sources.

ACKNOWLEDGMENT

The authors acknowledge support from EA Technology.

REFERENCES

1. S. E. Wright and B. Vuksanovic 1996 *Journal of Sound and Vibration* **190**(3), 565–585. Active control of environmental noise, I.
2. S. E. Wright and B. Vuksanovic 1997 *Journal of Sound and Vibration* **202**(3), 313–359. Active control of environmental noise, II.
3. B. Widrow and S. D. Stearns 1995 *Adaptive Signal Processing*, Englewood Cliffs NJ: Prentice-Hall.
4. S. J. Elliott, I. M. Stothers and P. A. Nelson 1987 *IEEE Transactions on Acoustics, Speech, and Signal Processing* **ASSP-35**, 1423–1434. A multiple error LMS algorithm and its application to the active control of sound and vibration.
5. S. J. Elliott, C. C. Boucher and P. A. Nelson 1992 *IEEE Transactions on Signal Processing* **40**, 1041–1052. The behaviour of a multiple channel active control system.
6. S. M. Kuo and D. R. Morgan 1996 *Active noise control systems: algorithms and DSP implementations*. New York: John Wiley & Sons, Inc.
7. P. F. Feinutch, N. J. Bershad and A. K. Lo 1993 *IEEE Transactions on Signal Processing* **41**, 1518–1531. A frequency domain model for "filtered" LMS algorithms—stability analysis, design and elimination of the training mode.
8. S. D. Snyder and C. H. Hansen 1994 *IEEE Transactions on Signal Processing* **42**, 950–953. The effect of transfer function estimation errors on filtered-X LMS algorithm.
9. S. J. Elliott and P. Darlington 1985 *IEEE Transactions on Acoustics, Speech, and Signal Processing* **33**, 715–717. Adaptive cancellation of periodic, synchonously sampled interference.
10. S. E. Wright and B. Vuksanovic 1999 *Journal of Sound and Vibration* (accepted for publication). Active control of environmental noise IV.

APPENDIX

Proof of equations (10), (13) *and* (14)

$$E = D + CW \tag{A1}$$

$$J = \Sigma |E|^2 = E^H E \tag{A2}$$

$$= W^H C^H C W + W^H C^H D + D^H C W + D^H D \tag{A3}$$

$$= W^H a W + W^H b + b^H W + C \tag{A4}$$

where $$a = C^H C \qquad b = C^H D \qquad C = D^H D \tag{A5}$$

For complex quantities

$$W = W_R + jW_I \qquad a = a_R + ja_I \qquad b = b_R + jb_I \tag{A6}$$

$$J = (W_R + jW_I)^H (a_R + ja_I)(W_R + jW_I) + (W_R + jW_I)^H (b_R + jb_I) + (b_R + jb_I)^H (W_R + jW_I) + C \tag{A7}$$

$$= W_T^T a_R W_R + W_I^I a_R W_I - 2W_R^T a_I W_I + 2b_R^T W_R + 2b_I^T W_I + C \tag{A8}$$

Generally it

$$u = X^T A X \qquad u = A^T X \qquad u = X_R^T A X_I \qquad u = X_R^T A X_I \tag{A9}$$

then $$\frac{\partial u}{\partial x} = 2Ax, \qquad \frac{\partial u}{\partial x} = A, \qquad \frac{\partial u}{\partial x_R} = AX_I, \qquad \frac{\partial u}{\partial x_I} = A^T X_R = -AX_R \tag{A10}$$

giving

$$\frac{\partial J}{\partial W_R} = 2a_R W_R - 2a_I W_I + 2b_R \qquad \frac{\partial J}{\partial W_I} = 2a_R W_I + 2a_I W_R + 2b_I \tag{A11}$$

$$\nabla J = \frac{\partial J}{\partial W_R} + j\frac{\partial J}{\partial W_I} \tag{A12}$$

$$\nabla J = 2a_R(W_R + jW_I) - 2a_I(W_I - jW_R) + 2(b_R + jb_I) \tag{A13}$$

$$= 2(a_R + ja_I)(W_R + jW_I) + 2(b_R + jb_I) \tag{A14}$$

$$= 2(aW + b) = 2C^H(CW + D) = 2C^H E \tag{A15}$$

(equation 10)

$$\nabla J = 0 \qquad aw_0 + b = 0 \qquad W_0 = -a^{-1}b = -(C^H C)^{-1} C^H D \tag{A16}$$

(equation 13)

Substituting in A4

$$J_0 = W_0^H a W_0 + W_0^H b + b^H W_0 + C \tag{A17}$$

$$= b^H W_0 + C = (C^H D)^H (-(C^H C)^{-1} C^H D) + D^H D \tag{A18}$$

$$= D^H [I - C(C^H C)^{-1} C^H] D \tag{A19}$$

(equation 14)